fractal and fractional

MDPI

Article

Bitcoin, Fintech, Energy Consumption, and Environmental Pollution Nexus: Chaotic Dynamics with Threshold Effects in Tail Dependence, Contagion, and Causality

Melike E. Bildirici [1], Özgür Ömer Ersin [2,*] and Yasemen Uçan [3,*]

[1] Department of Economics, Faculty of Economics and Administrative Sciences, Davutpaşa Campus, Yildiz Technical University, 34220 İstanbul, Türkiye; bildiri@yildiz.edu.tr or melikebildirici@gmail.com
[2] Department of International Trade, Faculty of Business, Sütlüce Campus, İstanbul Ticaret University, 34445 İstanbul, Türkiye
[3] Department of Mathematical Engineering, Faculty of Chemistry and Metallurgy, Davutpaşa Campus, Yildiz Technical University, 34210 İstanbul, Türkiye
* Correspondence: oersin@ticaret.edu.tr or ozgurersin@gmail.com (Ö.Ö.E.); ucan@yildiz.edu.tr (Y.U.)

Abstract: The study investigates the nonlinear contagion, tail dependence, and Granger causality relations with TAR-TR-GARCH–copula causality methods for daily Bitcoin, Fintech, energy consumption, and CO_2 emissions in addition to examining these series for entropy, long-range dependence, fractionality, complexity, chaos, and nonlinearity with a dataset spanning from 25 June 2012 to 22 June 2024. Empirical results from Shannon, Rényi, and Tsallis entropy measures; Kolmogorov–Sinai complexity; Hurst–Mandelbrot and Lo's R/S tests; and Phillips' and Geweke and Porter-Hudak's fractionality tests confirm the presence of entropy, complexity, fractionality, and long-range dependence. Further, the largest Lyapunov exponents and Hurst exponents confirm chaos across all series. The BDS test confirms nonlinearity, and ARCH-type heteroskedasticity test results support the basis for the use of novel TAR-TR-GARCH–copula causality. The model estimation results indicate moderate to strong levels of positive and asymmetric tail dependence and contagion under distinct regimes. The novel method captures nonlinear causality dynamics from Bitcoin and Fintech to energy consumption and CO_2 emissions as well as causality from energy consumption to CO_2 emissions and bidirectional feedback between Bitcoin and Fintech. These findings underscore the need to take the chaotic and complex dynamics seriously in policy and decision formulation and the necessity of eco-friendly technologies for Bitcoin and Fintech.

Keywords: chaos; fractionality; entropy; complexity; copula; threshold; TAR-TR-GARCH–copula causality; GARCH; causality; Fintech; bitcoin; energy consumption; environmental pollution

check for updates

Citation: Bildirici, M.E.; Ersin, Ö.Ö.; Uçan, Y. Bitcoin, Fintech, Energy Consumption, and Environmental Pollution Nexus: Chaotic Dynamics with Threshold Effects in Tail Dependence, Contagion, and Causality. *Fractal Fract.* **2024**, *8*, 540. https://doi.org/10.3390/fractalfract8090540

Academic Editors: Manashita Borah, Christos Volos and Norbert Herencsar

Received: 22 July 2024
Revised: 9 September 2024
Accepted: 16 September 2024
Published: 18 September 2024

Copyright: © 2024 by the authors. Licensee MDPI, Basel, Switzerland. This article is an open access article distributed under the terms and conditions of the Creative Commons Attribution (CC BY) license (https://creativecommons.org/licenses/by/4.0/).

1. Introduction

There is currently a large body of research looking into the possible chaotic structure of environmental pollution. Lorenz introduced a useful tool in 1963 to illustrate the dynamic characteristics of these kinds of systems [1]. Ruelle and Takens [2] showed that the structure of the atmospheric system is complex and nonlinear, with both deterministic and stochastic components [2]. Several papers have provided empirical evidence of chaotic features in average ozone concentrations. Guckenheimer and Holmes [3] explored nonlinear oscillations and bifurcations. Further atmospheric time series, including carbon dioxide (CO_2) and nitrogen dioxide (NO_2), are shown to follow Voltera–Wiener–Korenberg processes governed by high-dimensional chaos [4]. Using the Lyapunov exponents, evidence of chaotic structures has been discovered in major pollutants, including sulfur dioxide (SO_2), CO_2, NO_2, and particulate matter 10 (PM10) air pollution [5]. Impacts of time delay, chaos dynamics, and climate change on chaotic atmospheric propagation properties were identified with the Lorenz climate model updated with Caputo-type fractionality [6]. There have

been studies on the chaotic dynamics of air pollution in China, India, and Türkiye [7], as well as the use of Lie group algebra to study the chaotic dynamics of air temperature [8].

Studies investigating the chaotic nature of weather events, the atmosphere, and environmental pollution have not explored the relationship between the factors causing these events and their Granger causality. However, some other studies in the literature have specifically examined the relationship and causality between environmental pollution and the factors contributing to it. These studies generally utilized linear time series methods. In these works, energy consumption was considered a significant factor in atmospheric events and environmental pollution. The relationship between atmospheric events and energy consumption is based on the interaction of various factors, and this interaction can affect energy demand in both the short and long term. On the other hand, the relationship between atmospheric events and energy consumption is complex and is shaped by both short-term conditions and long-term conditions.

In this study, we will investigate Bitcoin and Fintech, which have been discussed in the recent literature as significant factors contributing to energy consumption (EC) and environmental pollution. Bitcoin's annual EC is estimated to range between 135 and 177 terawatt-hours (TWh) [9], resulting in a substantial carbon footprint [10], and the policies focusing on renewable energy will not solve the EC problem of Bitcoin [11]. However, the EC from Bitcoin is directly attributed to its cryptocurrency-mining algorithm, Proof of Work (PoW), and the high-level complex calculations requiring excessive energy use [12]. Recently, the daily EC of Bitcoin is predicted to be the equivalent of whole nations, such as Sweden and Thailand [13]. Bitcoin's peak annual energy usage is predicted as 204 terawatt-hours (TWh) of electricity [14]. An estimated 95 million tons of CO_2 emissions are produced annually as a result of this electro-intensive usage [9]. Additionally, every cryptocurrency transaction as a Fintech can add 619 kilowatt-hours (KWh) with a massive carbon footprint, and this amounts to EC resulting from 350,000 debit card transactions or 20.92 days' worth of EC for the average family in the United States [15]. This would surpass the annual carbon emissions of Qatar and the Czech Republic combined [16]. These results support the notion that Fintech and Bitcoin will continue to have a major influence on patterns of environmental pollution in the future [17].

The literature lacks exploration of the impacts of the recent developments in digital finance, mainly Bitcoin and Fintech, and the inclined use of EC contributing to the CO_2 emissions, as well as their chaotic structure with long-term dependence leading to nonlinearity in contagion and causality. The research explores how dependence, contagion, and Granger causality are revealed. To accomplish these goals, the study uses the threshold autoregressive-threshold-generalized autoregressive conditional heteroskedasticity–copula causality (TAR-TR-GARCH–copula causality) approach [18] to analyze a dataset of daily observations from 25 June 2012 to 22 June 2024. The reason for starting on 25 June 2012 is due to data limitations. Specifically, on 9 January 2009, the revised version of the software, Bitcoin 0.1, was released. In February 2011, Bitcoin reached parity with the U.S. dollar, with BTC 1 valued at USD 1. In April, Bitcoin began trading against the euro and the pound sterling. In 2012, the first halving occurred, reducing the reward per block from BTC 50 to 25. Therefore, we started the study on 25 June 2012.

The TAR-TR-GARCH–copula causality method [18] will provide essential tools for investigating causality, asymmetric behavior, persistence, and contagion effects between Bitcoin, Fintech, energy consumption, and environmental pollution simultaneously. This method employed in this study offers significant benefits by allowing each unique regime to exhibit varying characteristics, thereby facilitating the analysis of regime-specific contagion and causality behavior. Ignoring the outcomes of nonlinear regime-specific relationships and relying solely on conventional linear causality methods for policymaking could lead to inefficiencies in policy advocations. The method proves valuable in guiding researchers to devise policies tailored to the specific needs of different economic regimes. Through this approach, testing for mutual causality becomes feasible, aiding in discerning causality direction and status and assessing regime-specific Granger causality. Ultimately, identifying

causality remains a crucial tool for policymaking, particularly in the realm of environmental policy recommendations. These findings hold promise for offering relevant policy recommendations to policymakers.

This paper is organized into five main sections. Section 2 outlines the methodology, Section 3 presents the data and the empirical steps, Section 4 includes the empirical results, followed by discussion and policy implications, and Section 5 presents the conclusions.

2. Method

2.1. TAR-TR-GARCH

In the threshold autoregressive-threshold-generalized autoregressive heteroskedasticity (TAR-TR-GARCH) model, the conditional mean and conditional volatility process followed by a time series x_t is modeled as follows [18,19]:

$$x_t = \left(\alpha_0 + \sum_{p=1}^{p} \alpha_1 x_{t-p}\right) I(s_t < c) + \left(\beta_0 + \sum_{r=1}^{r} \beta_1 x_{t-r}\right) I(s_t \geq c) + \varepsilon_t \quad (1)$$

here, ε_t, the residual, is composed of two factors:

$$\varepsilon_t = \eta_t \delta_t \quad (2)$$

where, the first is η_t, a white noise process, and the second is δ_t, a nonlinear and heteroskedastic process that follows the nonlinear conditional volatility in each regime determined by an indicator function:

$$\delta_t^2 = \left(\omega_0 + \sum_{q=1}^{q} \omega_q \varepsilon_{t-q}^2 + \sum_{p=1}^{p} \vartheta_p \delta_{1,t-p}^2\right) I(s_t < c) + \left(\varsigma_0 + \sum_{q=1}^{q} \varsigma_q \varepsilon_{t-q}^2 + \sum_{p=1}^{p} \tau_p \delta_{t-p}^2\right) I(s_t \geq c). \quad (3)$$

Hence, combined with the conditional mean process given in Equation (1), the model in Equations (1)–(3) is denoted as a TAR-TR-GARCH(p,q) model with autoregressive conditional heteroskedasticity (ARCH) and generalized ARCH (GARCH) orders q and p, a threshold autoregressive (TAR) process in the mean, and a threshold generalized autoregressive conditional heteroskedasticity (TR-GARCH) in the conditional variance processes in two distinct regimes. Regimes are governed by the following:

$$\begin{aligned} I(s_t, c) &= 1 \; for \; s_t < c, \\ I(s_t, c) &= 0 \; for \; s_t \geq c. \end{aligned} \quad (4)$$

where $I(s_t, c)$ is the indicator function determining states depending on the distance between c, the threshold, and the transition variable, s_t, so that $s_t = x_t$ or lags of x_{t-i} for i = 1, 2, . . ., l; l is the maximum lag length determined with an information criterion, for instance, SIC, the Schwarz information criterion, known for parsimony [18,19]. Instead, one could allow the regime switches to be governed by the type of shocks distinguished among positive or negative ones by allowing $s_t = \varepsilon_{t-1}$ and $c = 0$ to achieve the following indicator function for two regimes:

$$\begin{aligned} I(\varepsilon_{t-1}) &= 1 \; for \; \varepsilon_{t-1} < 0, \\ I(\varepsilon_{t-1}) &= 0 \; for \; \varepsilon_{t-1} \geq 0. \end{aligned} \quad (5)$$

which determines the regime the process follows at each t for the sample $t = 1, 2, \ldots, T$ as a function of the type of shock at $t-1$ [18]. The portmanteau tests for threshold testing is well-established, and for optimum splitting of the regression space to sub-regression-spaces known as regimes, readers are referred to [20].

2.2. TAR-TR-GARCH–Copula

The method generalizes the TAR-TR-GARCH process that captures the marginals of data to copula for joint processes. The Symmetrized Joe-Clayton copula function is as follows:

$$F_{sjc}(v_1, v_2|\tau^v, \tau^L) = 0.5(F_{jc}(v_1, v_2\Big|\tau^U, \tau^L) + F_{jc}(1-v_1, 1-v_2\Big|\tau^U, \tau^L) + v_1 + v_2 - 1) \quad (6)$$

with upper and lower tails denoted by τ^v and τ^L, respectively [21]. F_{jc} is the Joe-Clayton copula:

$$F_{jc}(v_1, v_2|\tau^v, \tau^L) = 1 - \left(1 - \left\{\left[1-(1-v_1)^\kappa\right]^{-v} + \left[1-(1-v_2)^\kappa\right]^{-v} - 1\right\}^{-1/v}\right)^{-1/\kappa} \quad (7)$$

where, $\kappa = 1/\log_2(-2\tau^v)$, $v = -1/\log_2(\tau^L)$, and $\tau^v, \tau^L \in (0,1)$. The SJC copula captures the tail dependency at the lower and the upper tails with the condition of symmetry, $\tau^v = \tau^L$; however, this generalization assumes that asymmetry is rejected among lower and upper tail parameters [21].

2.3. Granger Causality Tests under Threshold-Type Nonlinear Heteroskedasticity

A recent study by J. M. Kim et al. [22] proposes the copula-based Granger causality (GC) method, which extends the traditional Granger causality framework introduced by Granger [23]. Bildirici et al. extended the MSGARCH–copula causality test [24], and this paper extends the copula augmented GC to the TAR-TR-GARCH–copula causality test. The null of no GC is tested with Equation (8):

$$f(b_{t+1}|b_t^n a_t^m) = f(b_{t+1}|b_t^n) \quad (8)$$

where $b_t^n = (b_t, \ldots, b_{t-n+1})$ and $a_t^m = (a_t, \ldots, a_{t-m+1})$ display previous information among B and A with n and m being their respective orders, and f is the conditional probability of the density function [25]. As a result, $f(b_{t+1}|b_t^n a_t^m)$ on the left side of Equation (8) reflects the predictability of B at period t + 1 with past information regarding both A and B time series given for period t. The right-hand side $f(b_{t+1}|b_t^n)$ assumes the prediction of B at t + 1 based on information regarding B itself at t. Therefore, the equality in Equation (8) shows that the bivariate setting's prediction performance is equivalent to that of the univariate one. Hence, to test H_0: A$\nrightarrow$B, i.e., no GC from A to B, against H_1: A$\mapsto$B, the alternative of GC running from A to B, the likelihood ratio test statistic is calculated:

$$GC_{A\to B} = E\left[\log \frac{f(b_{t+1}|b_t^n a_t^m)}{f(b_{t+1}|b_t^n)}\right] \quad (9)$$

which could be written as follows:

$$GC_{A\to B} = E\left[\log \frac{f(b_{t+1}|b_t^n a_t^m)}{f(b_{t+1}|b_t^n)}\right] = E\left[\log \frac{h(b_{t+1}, a_t^m|b_t^n)}{f(b_{t+1}|b_t^n) \times g(a_t^m|b_t^n)}\right] \quad (10)$$

which is the GC representation, where f and g are the marginal densities of B and A and h is the conditional joint density of (A, B). The conditional joint density is as follows [25]:

$$h(b_{t+1}, a_t^m|b_t^n) = f(b_{t+1}|b_t^n) \times g(a_t^m|b_t^n) \times c(u, v|b_t^n) \quad (11)$$

here, for $u = F(b_{t+1}|b_t^n)$ and $v = G(a_t^m|b_t^n)$, F and G represent conditional marginal distributions of B and A, and c is the copula density function. Using Equation (11) within Equation (10) leads to Equation (12):

$$CGC_{A\to B} = E[\log c(F(b_{t+1}|b_t^n)), G(a_t^m|b_t^n)|b_t^n] \quad (12)$$

$CGC_{A\to B}$ represents copula GC from A to B. Hence, the proposed approach incorporates nonlinearity in the context of threshold-based regime changes as an extension of [18] to copula.

3. Materials

3.1. Data

This paper uses a dataset that consists of daily observations for four variables—Bitcoin, Fintech, energy consumption, and global CO_2 emission concentrations in the air—and the sample covers 25 June 2012–22 June 2024. As noted in Section 1, with the acceptance of BTC in the U.S. dollar and euro-denominated financial markets after 2012, BTC transactions and volume grew drastically in size in the global financial markets as well as the cryptocurrency markets, in addition to the major halving event for Bitcoin in 2012, which justifies the choice of the period of the sample analyzed. BTC represents daily Bitcoin prices in USD and is obtained from Yahoo Finance. The energy consumption, denoted as EC, is measured by employing the Bitcoin Energy Consumption Index, available from the Cambridge Center for Alternative Finance, Cambridge University, which corresponds to the daily power demand of the Bitcoin network in terawatt-hours. Daily atmospheric carbon dioxide emission concentrations in the air, measured as particles per meter, are denoted as $CO_{2,}$ and the source is the CO_2 Earth Database. FIN represents the Global Fintech Index, and the data are obtained from the STOXX Database.

For BTC and EC, daily observations exist for all days of the period, including the weekends as well as for holidays. For CO_2, data are also available for weekends and holidays; however, there is a very low and negligible number of days with missing data for which no data are supplied from the database. For FIN, given that it represents an index of global Fintech firm stocks, data exist for working days as is expected for stock markets. To match observations, data for weekends and holidays are supplied. Afterward, missing observations for CO_2 are removed. Hence, the sample size utilized in the analyses becomes n = 3000. The level variables are subject to natural logarithms to reduce the size of outliers and obtain desired properties. Due to stationarity and unit root tests, the data are further first-differenced. Logarithmic and first differencing are also common in the literature to obtain the daily % changes of the variables.

As seen in Section 3, the method integrates a set of long-range dependence, fractionality, fractional difference parameter d estimations, and tests with various techniques. Also, variables are examined with a set of unit root and stationarity tests in Section 4. The overlook suggests that, for level series, the fractional difference parameters approach 1, a result in line with the unit root tests, which assume d = 1. Further, the nonlinear unit root tests given in Section 4 suggest that the level series are integrated in the order of 1, which cannot be rejected statistically. As a result, we conducted a set of descriptive statistics for the first-differenced series along with the level series.

Bitcoin, energy consumption, Fintech, and CO_2 emissions series, denoted as BTC, EC, FIN, and CO_2, respectively, are depicted in Figures 1–4 for their log-first differences for the analyzed period. The overlook suggests that all series are subject to volatility clustering, indicating that periods with low variance and dispersion tend to follow such periods, and after a shift to high variance periods, the periods of high variance prevail. BTC, EC, and FIN series are also subject to sharp outliers in specific periods. Nevertheless, such findings are also evident for $CO_{2,}$ and all series are subject to volatility clustering and sharp changes or regime shifts as well as certain outliers, especially those that occur during periods with relatively high variance.

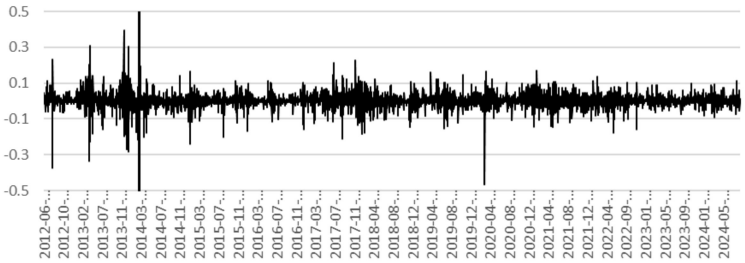


Figure 1. Bitcoin prices, daily % change. Source: Yahoo Finance, https://finance.yahoo.com/quote/BTC-USD/history/ (accessed on 29 August 2024).

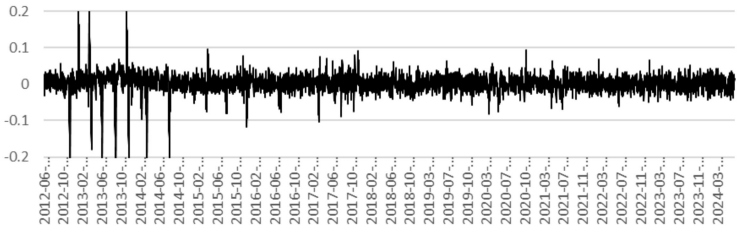


Figure 2. Energy consumption of Bitcoin network, daily % change. Source: Cambridge Center for Alternative Finance, Cambridge University, https://ccaf.io/cbnsi/cbeci (accessed on 29 August 2024).

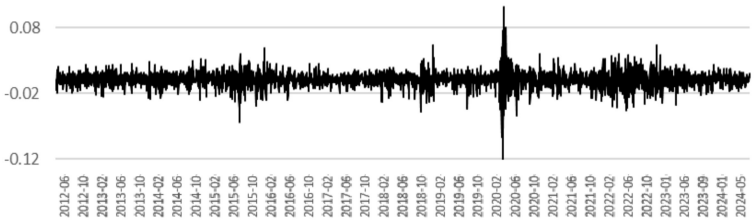


Figure 3. STOXX global fintech index, daily % change. Source: STOXX Global Fintech Index, https://stoxx.com/index/stxftgr/ (accessed on 29 August 2024).

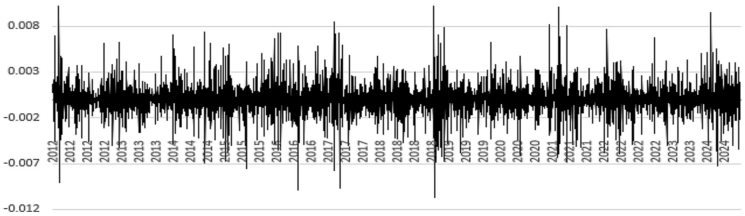


Figure 4. Global CO_2 emissions, daily % change. Source: Global Monitoring Laboratory, National Oceanic and Atmospheric Admin., https://gml.noaa.gov/ccgg/trends/data.html (accessed on 29 August 2024).

The descriptive statistics for level and first-differenced series are reported in Table 1. The results indicate very high kurtosis statistics, coupled with skewness statistics with negative values, especially for the first-differenced series, i.e., daily % changes. Excess kurtosis observed for Bitcoin and Fintech series indicates heavy tails and leptokurtic distribution due to heteroskedasticity. A relatively low level of kurtosis, but a significant level of skewness, is obtained for the CO_2 series, suggesting asymmetry in distribution. Skewness statistics also indicate strong skewness for Bitcoin and Fintech series. The null of normality is rejected with the JB test at conventional levels for the first-differenced series. Therefore, all series fail to follow normal distributions.

Table 1. Descriptive statistics.

	Variables in Levels				First Differences [1]			
	BTC	**EC**	**CO_2**	**FIN**	**ΔBTC**	**ΔEC**	**ΔCO_2**	**ΔFIN**
Mean	7.9469	0.6058	6.0138	5.8193	0.0021	0.0017	0.0000	0.0006
Med [2]	8.7626	1.4444	6.0142	5.9380	0.0013	0.0029	0.0000	0.0009
Max	11.1991	3.0222	6.0605	6.6272	1.4742	0.5131	0.0101	0.1107
Min	1.8406	−5.1985	5.9671	4.5915	−0.8488	−0.3710	−0.0106	−0.1388
SD	2.3526	2.0115	0.0218	0.5893	0.0522	0.0309	0.0016	0.0122
S	−0.5977	−0.9682	−0.0565	−0.4565	4.3700	−0.0766	0.1410	−0.5648
K	2.4713	3.1742	2.0624	1.9680	186.8476	45.1815	8.4050	14.8286
JB	311.90	690.01	143.10	243.9158	6,183,840.0	324,796.0	4700.3	18,137.2
p	0.0000	0.0000	0.0000	0.0000	0.0000	0.0000	0.0000	0.0000

[1] Δ denotes first differencing or, equivalently, $d = 1$. [2] Med is the median, JB is the chi-square test statistic for the Jarque–Bera test of H_0: series is normally distributed, and *p* is its probability. SD is standard deviation, and S and K are skewness and kurtosis, respectively.

The findings in Table 1 are in line with Figures 1–4, which provide insights into excess kurtosis, asymmetry, volatility clustering for the series analyzed and possibly nonlinearity in the series. These findings are confirmed by the skewed distributions, excess kurtosis, and the JB test results, which point to the non-normality of the series evaluated.

3.2. Empirical Stages

The empirical stages consist of the following four stages. The first 3 focus on long-run dependence, fractionality, nonlinearity, and chaotic dynamics. The 5th stage focuses on modeling contagion and causality dynamics.

i. Long-term Dependence and Fractionality. Long-term dependence is examined with two rescaled range (R/S) tests. Fractional difference parameters are measured with two different methods. The tests are conducted with robust methods for heteroskedasticity and autocorrelation. These tests include the following:

- Hurst–Malderbrot R/S test [26–28] and Lo's R/S test [29] for long-run dependence.
- Covariance matrices of both R/S tests are conducted with Andrews' method [30] for heteroskedasticity and autocorrelation-consistent covariances.
- Long-memory and fractional differentiation parameter d is estimated and tested with Geweke and Porter-Hudak [31] and Phillips' estimators [32].

ii. Largest Lyapunov Exponents, Chaotic Dynamics, Entropy, and Complexity.

- Series are evaluated with Shannon [33], Rényi [34], and Tsallis [35] entropy, which generalizes Havrda–Charvât entropy (HCT) [35,36]. The Tsallis entropic q index is calculated [37] and evaluated for varying q to examine changes in entropy once q is altered.
- Complexity is tested with Kolmogorov–Sinai complexity [38].
- Hurst exponents are estimated for the determination of chaos, Brownian motion, and mean reversion.
- The largest Lyapunov exponents are calculated with two methods, Kantz [39] and Rosenstein–Collins–DeLuca [40]. Both methods found profound applications in the measurement of the largest Lyapunov exponent (λ). As a rule of thumb, the λ results give information on the average exponential rate of phase-space divergence or convergence of neighboring orbits.
  - $\lambda > 0$ specifies chaos; $\lambda \leq 0$ regular motion; $\lambda < 0$ a bifurcation; and $\lambda > 1$ deterministic chaos.
  - In the case of $\lambda \leq 0$ or $\lambda > 1$, copula Granger causality tests are not explored.
  - However, when $0 < \lambda < 1$, and Shannon, HCT, Tsallis, Rényi, and Kolmogorov–Sinai measures yield a positive value, and findings suggest an acceptable degree of uncertainty or random processes.

iii. Nonlinearity Testing.

- Brock et al.'s [41] BDS test is used for independence and nonlinearity.
- Stationarity is tested with the KPSS [42], and the test is based on correlation dimensions and is accepted as being robust to structural breaks and nonlinearity.
- Unit root behavior is further tested with the nonlinear unit root test of Kapetanios et al., known as the KSS test [43].

iv. Modeling of Nonlinear Contagion, Tail Dependence, and Granger Causality.

- If the variables are stationary, the TAR-TR-GARCH–copula causality method will be applied to model contagion and causality behavior in the context of copulae for tails of the dataset.
- Nonlinear heteroskedasticity in marginal processes is modeled with TAR-TR-GARCH models.
- Joint distributions are modeled with asymmetric and regime-dependent copula functions with TAR-TR-GARCH–copula.
- Causality testing is performed with TAR-TR-GARCH–copula causality tests.

4. Results

4.1. Long-Term Dependence and Fractionality

In this section, the series will be tested for long memory using Lo's [26,27,29] and Hurst–Mandelbrot R/S tests [26,27,29]. The results are presented in Table 2.

Table 2. R/S Tests and fractional difference parameter estimation results.

Variables in Levels				
Statistics:	**BTC**	**EC**	**CO_2**	**FIN**
Hurst–Mandelbrot's R/S [1]	28.7 ***	28.0 ***	25.9 ***	24.3 ***
Lo's modified R/S	3.07 ***	3.07 ***	3.01 ***	2.77 ***
d parameter (GPH) [2]	0.963081 ***	1.0178 ***	0.966206 ***	1.0261 ***
t statistic	24.0699	17.7349	21.1036	25.6480
p, H_0: d = 0	0.000	0.000	0.000	0.000
d parameter (Phillips)	0.9948 ***	0.9173 ***	0.9229 ***	0.8981 ***
t statistic	11.8826	10.8852	7.5987	9.5373
p, H_0: d = 0	0.000	0.000	0.000	0.000
First-differenced				
Hurst–Mandelbrot's R/S	1.32	2.39 ***	0.346	1.08
Lo's modified R/S	1.31	1.32	0.345	1.07
d parameter (GPH)	0.087555	−0.117578	0.055637	−0.024553
t statistic	1.0892	−1.4941	0.4575	−0.2507
p, H_0: d = 0	0.280	0.140	0.649	0.803
d parameter (Phillips)	0.0641901	−0.002346	0.1021 *	0.1067214
t statistic	0.7869	−0.0255	1.95225	0.9322
p, H_0: d = 0	0.434	0.980	0.000	0.355
Volatility				
Hurst–Mandelbrot's R/S	2.16 ***	4.84 ***	2.21 ***	3.96 ***
Lo's modified R/S	1.88 **	2.3 ***	1.55	1.74 *
d parameter (GPH)	0.059604 **	0.095537 *	0.290907 ***	0.165445 ***
t statistic	2.3613	1.6936	3.1380	5.6241
p, H_0: d = 0	0.021	0.095	0.003	0.000
d parameter (Phillips)	0.0130452	0.0519135	0.4856908 ***	0.1805063 ***
t statistic	0.5085	0.9739	5.3014	6.1596
p, H_0: d = 0	0.613	0.334	0.000	0.000

[1] The critical values in R/S tests are as follows. 90%: [0.861, 1.747], 95%: [0.809, 1.862], and 99%: [0.721, 2.098]. [2] d (GPH) and d (Phillips) are the Geweke and Porter-Hudak's [31] and Phillips' [32] long-memory (fractional integration) parameters. *, **, *** indicate statistical significance at 10%, 5% and 1% levels of statistical significance, respectively.

In both tests, heteroskedasticity and autocorrelation robust covariance methods from [30] are employed. In both R/S tests, the null hypothesis is: "H_0: variable is not long-range dependent". Phillips' method augments Geweke and Porter-Hudak's estimator to achieve robust results in the case of series with d > 1. The tests are conducted for level series followed by series in the first differences and the volatility series in the last section of Table 2. For all variables in levels, Hurst–Mandelbrot R/S and Lo's modified R/S tests suggest evidence of long-range dependence at a 1% level of statistical significance. Afterward, the fractional difference parameter, d, is estimated with Geweke and Porter-Hudak [31] (henceforth, GPH) and Phillips' methods [32]. An overlook suggests that fractional difference parameters are statistically significant for all level series in addition to being in the range of 0.90 to 1.02. As typical, for BTC, the GPH estimate for d is 0.963, and the Phillips estimate is 0.9948, and for EC, the estimates are 1.0178 and 0.9173 with the respective methods. For CO_2, the parameter d is estimated as 0.966 and 0.9229 with these methods, respectively. For FIN, the fractional difference parameter is estimated as 1.0261 and 0.8981 with the respective estimators.

In the second section of Table 2, the variables are first-differenced, i.e., d is taken as 1 for all series. Since the level series are subject to logarithms, once first-differenced, the first-differenced series reflect their respective daily % changes. For Hurst–Mandelbrot's test, long-range dependence is rejected for the majority of the series except for EC. For all series, Lo's modified R/S test indicates the insignificance of long-range dependence. Parameter d is estimated with GPH and Phillips' methods, which also test H0: d = 0. The results yield the non-rejection of the null hypothesis for all series with both methods at a 1% significance level. One exception is the result of Phillips' method, which points to the statistical significance of the fractional differentiation parameter. However, this finding is statistically significant at a 10% level of significance only, while being insignificant at the conventional 5% significance level.

According to the descriptive tests presented in Table 1, the variables showed signs of heteroscedasticity as evident with excess kurtosis and as to be shown in the next section, and this suspicion is confirmed by ARCH Lagrange multiplier (ARCH-LM) tests [44], which assesses ARCH-type heteroskedasticity. As a result, we also evaluated the volatility series for the series analyzed with the tests conducted for the series in levels and first difference. The results for the volatility series are given in the last part of Table 2. Following the literature, the volatility series are proxied by the daily realized variances. For all volatility series, Hurst–Mandelbrot's R/S test results also confirm the existence of long-range dependence. Lo's test confirms long-range dependence results for all series except CO_2, for which long-range dependence cannot be accepted statistically. The GPH and Phillips' methods point to the rejection of the null hypothesis that d = 0 for all volatility series, and the GPH method confirms the necessity of fractional differentiation for all series at a 5% level of significance except for EC and at a 10% significance level for EC. The Phillips estimator confirms the significance of fractional difference parameters for FIN and CO_2, while it rejects it for BTC and EC. The overall results suggest evidence of long-range dependence and fractionality, and variables are examined for chaos and entropy in the next section.

4.2. Lyapunov Exponent Results

After non-normality and fractionality tests, the analysis concentrated on the chaotic structure. Two methods were employed for estimating the Lyapunov exponents (λ): the methods in [39,40]. The rationale behind using two different methods stems from the recognition that although both methods are highly regarded, they may yield divergent results. Moreover, employing two methods serves as a precautionary measure and provides validation for the presence of chaos in the series if detected. The results are given in Table 3.

Table 3. Lyapunov exponent results.

	BTC	EC	CO_2	FIN
Kantz [39] [1]	0.88 ***	0.56 ***	0.69 ***	0.45 ***
Rosenstein et al. [40]	0.56 ***	0.556 ***	0.59 ***	0.42 ***

[1] Results for only one dimension are reported. Negative vx are obtained for the remaining dimensions. *** indicates significance at the 1% statistical significance level.

Both methods have demonstrated good performance in detecting chaotic processes even in the presence of noise. The main parameter, the embedded dimension, was set with three initial states. The results from the two methods focus solely on one dimension. Notably, the values of the Lyapunov exponent determined by the Kantz and Rosenstein et al. methods yielded different results; however, the results demonstrate the presence of chaotic dynamics in Bitcoin, its energy consumption, CO_2 emissions, and Fintech. A positive value of λ indicates a chaotic process, implying relatively low predictability of the series' trajectory. If λ is close to zero, the existence of chaotic behavior is considered fragile. Conversely, a negative value of λ strongly suggests the absence of chaotic behavior in the long run. The results obtained from the Kantz method yielded unexpected outcomes as the dimensions were varied from 1 to 3 for the selected variables. However, this discrepancy was not observed with the Rosenstein et al. method. Clear indications of chaos were observed for all variables, particularly for the environmental variable, where positive Lyapunov estimates ranged from 0.42 to 0.88. Thus, we conclude that all variables possess chaotic dynamics.

4.3. Kolmogorov Entropy Results

Kolmogorov entropy (KE) serves as a measure of the degree of information falsification [18]. This entropy, denoted as KE, can be calculated using two methods: the Lyapunov exponent and the correlation integral [25]. The first method involves deriving all positive Lyapunov exponents. In the case of the Bitcoin prices analyzed, the small yet positive values of entropy indicate that market information contributes to understanding market dynamics. If a variable is non-complex and entirely predictable, KE approaches zero. Conversely, when data are random, the value of KE is large and positive. A lower KE value suggests a more predictable structure within the series. Higher values indicate greater complexity. The results are presented in Table 4. Accordingly, KE is calculated as 0.39 and 0.50 for BTC and FIN and as 0.44 and 0.59 for EC and $CO_{2,}$ respectively. The results indicate that the Eckman–Ruelle condition is met for all variables and a moderate level of complexity exists for all variables, indicating that data are random and exhibit chaotic dynamics.

Table 4. Results of Kolmogorov entropy.

	Kolmogorov Entropy	Eckman–Ruelle Condition Satisfied?	Chaotic?
BTC	0.39	YES	YES
FIN	0.50	YES	YES
EC	0.44	YES	YES
CO_2	0.59	YES	YES

4.4. Shannon Entropy, Kolmogorov–Sinai Complexity, and Hurst Exponent Results

Furthermore, statistical techniques are effectively used to determine the complexity of nonlinear systems with Shannon entropy. Shannon entropy measures the rate of information generation in a system. To examine chaotic dynamics, Shannon entropy results are reported in the first column of Table 5. For robustness of the results, Rényi and HCT entropy results are presented in the second column. Kolmogorov–Sinai (KS) complexity measure and Hurst exponents are reported in the last two columns, respectively.

Table 5. Shannon, HCT, and Rényi entropy, Kolmogorov–Sinai complexity, and Hurst exponents.

	Shannon	1/Shannon	Rényi	HCT [1]	Kolmogorov–Sinai Complexity	Hurst Exponent
Variables in levels						
BTC	2.2891	0.4368	2.2941	3.5770	11.3929	0.9987
EC	3.8818	0.2576	2.4311	8.3719	12.0114	0.9984
CO_2	2.3026	0.4343	2.3190	3.5791	8.6387	0.9973
FIN	2.3010	0.4346	2.3015	3.5311	11.1691	0.9978
Variables in first differences (daily % change)						
BTC	4.3285	0.2310	1.2276	18.0076	11.8264	0.5706
EC	3.9269	0.2547	1.2166	17.3454	12.0363	0.5992
CO_2	11.9356	0.0838	1.4681	38.3030	11.7285	0.2627
FIN	4.6180	0.2165	1.2660	17.8724	11.5713	0.4872
Volatility series (daily realized variance)						
BTC	0.6557	1.5251	0.8115	4.2355	11.7519	0.9006
EC	0.7356	1.3594	0.8498	4.8556	12.0335	0.9255
CO_2	0.8321	1.2017	0.8860	5.3459	11.6088	0.7805
FIN	0.8277	1.2082	0.8923	5.1616	11.5638	0.8513

[1] Tsallis entropy measure [35] was developed by Tsallis in 1988 as a generalization of Havrda–Charvât entropy [36] and is denoted as HCT. Rényi is the Rényi entropy [34]. Both Rényi and HCT entropies are reported for default q values. HCT and Rényi entropies are calculated in STATA 16. Kolmogorov–Sinai complexity and Hurst exponent measures are calculated in MATLAB 2023b.

The Shannon entropy findings reveal a considerable degree of uncertainty, as indicated by all values being distinct from zero. Entropy also measures the information distortion reflected by EC, BTC, FIN, and CO_2, with positive entropy levels indicating the potential to understand the dynamics of these variables using associated information. Given that Shannon entropy values significantly exceed zero, the results confirm a significant degree of uncertainty in EC, BTC, FIN, and CO_2. Additionally, the variables were reanalyzed using the Rényi and HCT entropy measures, which validate the Shannon entropy's findings.

Furthermore, the variables were examined for their dependence on chaos, unpredictability, complexity, and beginning conditions using the Kolmogorov–Sinai complexity metric. This metric provides information on the degree of complexity and unpredictability in addition to the existence of chaos. Higher values of the Kolmogorov–Sinai complexity measure, which measures a system's complexity or unpredictability, may be seen as a sign of unpredictability because of the chaotic nature of the series [25]. We applied the Kaspar and Schuster approach to compute the Kolmogorov–Sinai complexity measure [45].

The KS complexity measure, in contrast to the Shannon and HCT measures for entropy, concentrates on certain features of the series. While KS entropy focuses on the predictability of trajectories and the behavior of dynamic systems, Shannon entropy is more concerned with probability distributions and information. As a result, while KS entropy is more interested in the dynamic characteristics of systems and their sensitivity to beginning conditions, Shannon entropy measures the information content of a source or distribution. Ultimately, the findings of the KS metric validate chaotic dynamics and randomness in addition to complexity, and the BTC, EC, FIN, and CO_2 series under analysis show unpredictability and chaotic behavior according to the findings of the Shannon, HCT, and KS measures.

Hurst exponents are examined for the variables analyzed in the last column of Table 5. The table provides the Hurst exponents for three distinct variable types: variables in levels, in first-differences, and the volatility series. The Hurst exponents for variables in levels are 0.9987, 0.9984, 0.9973, and 0.9978 for FIN, BTC, EC, and CO_2, respectively, and these values are all extremely near 1, suggesting a significant level of persistence. The Hurst exponents for the first-differenced series for BTC, EC, CO_2, and FIN are 0.5706, 0.5992, 0.2627, and 0.4872, respectively, and the findings suggest that CO_2 and FIN have a propensity towards mean reversion or anti-persistence, whereas the values of BTC and EC are above 0.5, indicating a random walk behavior.

The Hurst exponents for the volatility series are over 0.5 and are close to 1. Specifically, the exponents calculated for BTC and EC are 0.9006 and 0.9255, respectively, versus 0.7805 and 0.8513 for CO_2 and FIN, respectively. Consequently, the volatility series' Hurst exponents attest to the presence of long-term positive autocorrelation and persistence, meaning that periods of high (low) volatility are probably going to be followed by periods of high (low) volatility. The findings indicate that there is a mixed behavior for series in first differences with mean reversion tendencies and extremely persistent structures for levels series and volatility. Overall, the results for Bitcoin, Fintech, energy consumption, and air pollution demonstrate departures from their long-term equilibrium, as well as a noticeable and perceptible rise in uncertainty in these variables along with a decrease in the amount of information carried, and these findings point to uncertainty and randomness in all variables that were examined.

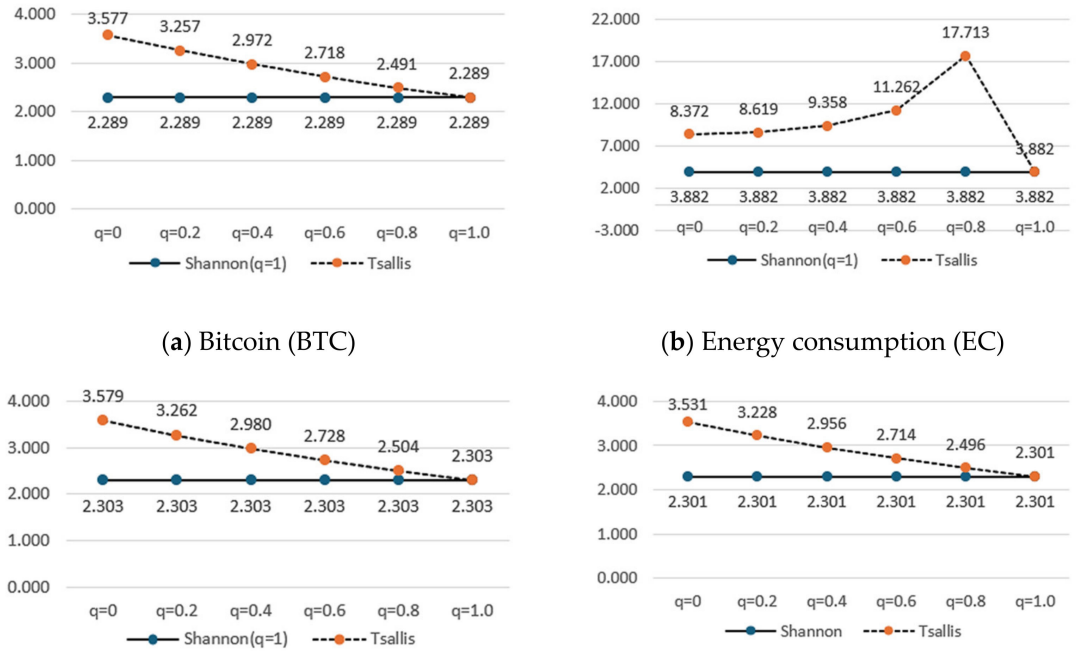
The Tsallis entropic index is utilized to characterize the behavior of the Tsallis entropy under varying q to test the sensitivity of the results for altered q. The results are given in Table 6. Table 6 also reports Shannon entropy results for comparative purposes. As for theoretical expectations, Tsallis entropy results converge Shannon for q = 1 reported in the last row. It should be noted that various q indices are proposed for financial series such as BTC and FIN, and different than the literature such as [46], the test cannot be altered for different conditions since the dataset is real data and a controlled experiment cannot be conducted.

Table 6. Tsallis entropic index for varying q and Shannon entropy.

			BTC			
Entropy [1]	q = 0	q = 0.2	q = 0.4	q = 0.6	q = 0.8	q = 1.0
Tsallis	3.577	3.257	2.972	2.718	2.491	2.289
Shannon (q = 1)	-	-	-	-	-	2.289
			EC			
	q = 0	q = 0.2	q = 0.4	q = 0.6	q = 0.8	q = 1.0
Tsallis	8.372	8.619	9.358	11.262	17.713	3.882
Shannon (q = 1)	-	-	-	-	-	3.882
			CO_2			
Tsallis	3.579	3.262	2.980	2.728	2.504	2.303
Shannon (q = 1)	-	-	-	-	-	2.303
			FIN			
Tsallis	3.531	3.228	2.956	2.714	2.496	2.301
Shannon	-	-	-	-	-	2.301

[1] Tsallis entropy is calculated for q = 0, 0.2, . . ., 0.8, and 1, with increments of 0.2 to save space. Similar to Rényi entropy, Tsallis entropy converges to Shannon entropy for q = 1.

For comparative purposes, Shannon entropy for q = 1 is presented in the second row, followed by the Tsallis entropic index for varying q. The results are also depicted in Figure 5a–d below along with Shannon entropy for the examined variables. The overlook of results in Table 6 and Figure 5a–d indicate that there is sensitivity to changes in q, reflecting varying levels of complexity and uncertainty across entropic index q; however, the index remains significantly positive for all cases, indicating complexity and variability of the data distributions.



(**a**) Bitcoin (BTC)

(**b**) Energy consumption (EC)

(**c**) CO_2 Emissions (CO2)

(**d**) Fintech (FIN)

Figure 5. Tsallis entropy for varying entropic index q and Shannon entropy with fixed q = 1.

BTC results are reported in the first part of Table 6 along with Figure 5a. Tsallis entropy is calculated as 3.577 for q = 0 for BTC, decreases as q increases from 0 to 1, and remains strictly positive for varying q, reflecting uncertainty or diversity in the data distribution. As the order q of Tsallis entropy reaches q = 1, Tsallis entropy equals 2.289, which matches the Shannon entropy. For EC, Tsallis entropy exhibits a non-monotonic pattern, starting at 8.372 at q = 0, increasing sharply at higher q, especially for q = 0.8, and then decreasing at q = 1, which suggests that EC data have a complex distribution that responds sensitively to changes in q.

For CO_2, Tsallis entropy equals 3.579 for q = 0, which decreases as q increases; however, the strict positivity remains significant as it reduces to 2.303 for q = 1, suggesting a limited reduction. For FIN, Tsallis entropy is 3.531 for q = 0, remains positive for different q, and diminishes as q increases. However, the complexity in the FIN time series cannot be rejected, since the index remains significantly positive as it reaches 2.301 for q = 1, demonstrating the expected convergence to the Shannon entropy.

The findings indicate that data distributions for BTC, EC, CO_2, and FIN have distinct complexity and variability characteristics, which are crucial for understanding their dynamic behavior and potential impacts on BTC and FIN market volatility as well as on EC and CO_2, with possible tail dependence and contagion and causality relations between the variables.

4.5. Specific Relationships between Fractionality, Chaos, and Entropy Measures

Fractionality, entropy, and chaos measures have specific relationships, and the tests utilized to examine these measures capture distinct aspects of system dynamics. Chaos indicators assess sensitivity and instability, entropy indicators quantify randomness and information content, and fractionality indicators provide insights into long-range dependence and predictability [7,39]. Time series with higher fractionality and long memory often exhibit lower entropy due to increased predictability from long-range dependence. However, this relationship is not absolute; nonlinear and complex systems may show high entropy even when fractionality is present, particularly if chaotic components are involved [47]. In the context of chaos, chaotic systems generally are characterized by high entropy as a result of their sensitivity to initial conditions and inherent unpredictability.

Importantly, a fractional time series does not necessarily exhibit chaos; while fractionality indicates correlations over time, chaos pertains to sensitivity to initial conditions [26]. Nonetheless, some fractional processes may exhibit chaotic behavior, as evidenced by positive Lyapunov exponents and associated higher Kolmogorov entropy, indicating chaotic dynamics [48].

By examining the results of the fractionality, chaos, and entropy measures collectively, considering positive largest Lyapunov exponents; significantly positive Hurst exponents; Shannon, Tsallis, and Rényi entropy measures indicating high uncertainty; and fractionality results obtained with Lo's and Hurst and Mandelbrot's tests along with GPH and Phillips' fractional integration parameter estimates, the findings indicate a complex relationship between predictability, randomness, and sensitivity in all series examined. The results are in line with [49] for the measures of complexity, and this comprehensive testing approach conducted in this study confirms the simultaneity of the presence of chaos, entropy, long-range dependence, and fractionality in the analyzed series, offering a nuanced understanding of the system's behavior.

4.6. Nonlinearity Testing

The BDS test utilizes correlation dimensions to assess independence under the null hypothesis, contrasting it against the alternative of nonlinearity and dependence. The findings are presented in Table 7. The BDS test results are given in two sub-sections: the first is the variables in levels, followed by the second set of results for variables in first differences. The test results indicate nonlinearity in all variables in levels and in first differences.

Table 7. BDS test results.

Variables in Levels								
	BTC		**CO_2**		**FIN**		**EC**	
Dim. [1]	**BDS**	**se**	**BDS**	**se**	**BDS**	**se**	**BDS**	**se**
2	0.2064 ***	0.0008	0.1971 ***	0.0007	0.2046 ***	0.0009	0.2069 ***	0.0012
3	0.3510 ***	0.0013	0.3362 ***	0.0011	0.3484 ***	0.0013	0.3514 ***	0.0018
4	0.4522 ***	0.0015	0.4333 ***	0.0013	0.4493 ***	0.0016	0.4521 ***	0.0021
5	0.5229 ***	0.0016	0.5010 ***	0.0014	0.5200 ***	0.0017	0.5220 ***	0.0022
6	0.5721 ***	0.0015	0.5479 ***	0.0013	0.5694 ***	0.0016	0.5704 ***	0.0021
Variables in First Differences								
Dim.	**BDS**	**se**	**BDS**	**se**	**BDS**	**se**	**BDS**	**se**
2	0.0255 ***	0.0017	0.0229 ***	0.0017	0.0221 ***	0.0016	0.0358 ***	0.0013
3	0.0490 ***	0.0027	0.0408 ***	0.0027	0.0446 ***	0.0026	0.0570 ***	0.0020
4	0.0647 ***	0.0032	0.0524 ***	0.0032	0.0609 ***	0.0031	0.0665 ***	0.0024
5	0.0742 ***	0.0033	0.0578 ***	0.0033	0.0693 ***	0.0032	0.0686 ***	0.0025
6	0.0790 ***	0.0032	0.0582 ***	0.0032	0.0729 ***	0.0031	0.0657 ***	0.0025

[1] Dim. represents the dimension of the BDS test, BDS is the BDS test statistic, and se is the standard error. *** designates statistical significance at 1% level of significance.

4.7. ARCH-Type Heteroskedasticity, Nonlinear Stationarity, and Unit Root Tests

Following the affirmation of nonlinearity, the analysis assesses ARCH-type heteroskedasticity and nonlinear stationarity and unit root tests. The findings are documented in Table 8. The presence of an ARCH effect is a prerequisite for applying ARCH-type models. The ARCH-LM tests are conducted at order 1, as well as at orders 1 through 5, in line with the standard practice observed in the literature, considering that the variables are based on working days in the sample.

In the second part of Table 8, variables are tested with the KPSS stationarity test. The test is known for producing robust results under structural breaks and nonlinearity. Further, the KSS test tests nonlinear unit root processes as an augmentation of the traditional linear augmented Dickey–Fuller test. KPSS test results indicate non-stationarity of all series in levels and stationarity in first-differenced series. For the level series, the nonlinear KSS test results show that the series follow unit root behavior. The tests are repeated after first differencing to examine possible changes in stationarity. The results indicate that all series follow nonlinear stationary processes once first-differenced.

Table 8. ARCH effects, KPSS stationarity, and KSS nonlinear unit root tests.

Level Series				
Test: [1]	**BTC**	**CO_2**	**FIN**	**EC**
ARCH-LM (1)	1895.42 ***	845.12 ***	5129.12 ***	904.22 ***
ARCH-LM (1–5)	952.11 ***	682.14 ***	4486.85 ***	592.46 ***
Result:	ARCH effects	ARCH effects	ARCH effects	ARCH effects
KPSS	7.4773	7.1541	6.7159	7.2480
Result:	Non-stationary	Non-stationary	Non-stationary	Non-stationary
KSS	−1.9766	−0.9064	−1.0263	−2.3848 *
Result:	Nonlinear unit root	Nonlinear unit root	Nonlinear unit root	Nonlinear unit root
First-Differenced Series				
	BTC	**CO_2**	**FIN**	**EC**
ARCH-LM (1)	7.9214 **	288.8419 ***	473.1748 ***	1903.0540 ***
ARCH-LM (1–5)	118.2135 ***	63.3936 ***	207.0430 ***	397.9321 ***
Result:	ARCH effects	ARCH effects	ARCH effects	ARCH effects
KPSS	0.3071 ***	0.0162 ***	0.2629 ***	0.2196 ***
Result:	Stationary	Stationary	Stationary	Stationary
KSS	−26.1182 ***	−25.1553 ***	−12.6214 ***	−9.4215 ***
Result:	Stationary	Stationary	Stationary	Stationary

[1] *, **, *** indicate statistical significance at 10%, 5% and 1% levels of statistical significance, respectively.

It should be noted again that the indication of ARCH effects across all tested series serves as the foundation for constructing models that account for conditional variance. When considering the results from Table 8 and the BDS test outcomes from Table 7 together, these findings provide a rationale for modeling BTC, Fintech, energy consumption, and CO_2 series with models that aim at capturing nonlinearity and ARCH-type heteroskedasticity dynamics in the series to be modeled.

4.8. The TAR-TR-GARCH–Copula Model Estimation Results

As outlined earlier, the TAR-TR-GARCH models introduce a threshold-based nonlinearity in both the conditional mean and variance processes. The optimal lag length, denoted as d, ranges from 1 to 5, adjusted based on the explanatory capacity of the models. Unlike the GARCH(1,1) model, these models distinguish between the effects of positive and negative shocks through an indicator variable. The estimation results are presented in Table 9.

The TAR-TR-GARCH model offers valuable insights into conditional tail dependence, providing key metrics to analyze how variables behave during extreme fluctuations. The results exhibit the signs and significance of estimated parameters for the TAR-TR-GARCH model, aligning with expected marginal density distributions. This study highlights the utility of generalizing copula-based distributional aspects for characterizing co-movements among the evaluated series. Additionally, estimation outcomes indicate significant asymmetric effects on volatilities within the series.

The model estimated for BTC is presented in columns 1 and 2 for regimes 1 and 2, followed by the models estimated for FIN, EC, and CO_2. In all models and all regimes, the ARCH and GARCH parameters are statistically significant at conventional levels of

statistical significance in addition to the constant parameters. The threshold parameter is estimated as 0.04085 for the model for BTC, whereas the threshold estimates are estimated as 0.038145, 0.0314, and 0.0254 for models for FIN, EC, and CO_2, respectively. Further, the stability condition, the sum of ARCH + GARCH < 1, is satisfied in both regimes for all models. The threshold mechanism successfully splits the regression space into two sub-spaces, the former being the low volatility and the latter being the high volatility. As typical, the threshold parameter is estimated as 0.04085 for the model of BTC, indicating that the positive shocks at and above the threshold value of 0.04085 generate a regime change from low- to high-volatility regimes, whereas for shocks below 0.04085, the low variance regime prevails.

Table 9. TAR-TR-GARCH–copula model estimation results.

Conditional Mean Process								
	BTC		**FIN**		**EC**		**CO_2**	
Regimes:	1	2	1	2	1	2	1	2
Const.	0.31 ***	0.456 ***	0.284 ***	0.42 ***	−0.09 ***	0.12 ***	0.29 ***	0.33 ***
p	(0.00)	(0.00)	(0.000)	(0.001)	(0.00)	(0.00)	(0.00)	(0.00)
AR(1)	0.105 ***	0.173 ***	0.097 ***	0.19 ***	0.105 ***	0.173 ***	0.093 ***	0.065 ***
p	(0.00)	(0.00)	(0.00)	(0.04)	(0.00)	(0.00)	(0.00)	(0.00)
Conditional Variance Process								
Const.	0.0448 ***	0.123 ***	0.0360 ***	0.118 ***	0.068 ***	0.147 ***	0.113 ***	0.155 ***
p	(0.00)	(0.000)	(0.00)	(0.01)	(0.00)	(0.00)	(0.00)	(0.00)
ARCH	0.13 ***	0.13 ***	0.22 ***	0.28 ***	0.26 ***	0.161 ***	0.311 ***	0.271 ***
p	(0.00)	(0.00)	(0.00)	(0.00)	(0.00)	(0.00)	(0.00)	(0.00)
GARCH	0.74 ***	0.79 ***	0.69 ***	0.68 ***	0.681 ***	0.801 ***	0.657 ***	0.682 ***
p	(0.00)	(0.00)	(0.00)	(0.00)	(0.00)	(0.00)	(0.00)	(0.00)
Threshold	0.04085 ***		0.038145 ***		0.0314 ***		0.0254 ***	
p	(0.00)		(0.00)		(0.00)		(0.00)	
Stability condition [1]	Yes	Yes	Yes	Yes	Yes	Yes	Yes	Yes
Copula Results: (SJC Copula)								
	BT-EC				FIN-EC			
Regimes:	1		2		1		2	
Lower	0.81 ***		0.831 ***		0.807 ***		0.818 ***	
Upper	0.84 ***		0.873 ***		0.806 ***		0.861 ***	
	BT-FIN				BT-CO_2			
Regimes:	1		2		1		2	
Lower	0.707 ***		0.82 ***		0.697 **		0.87 ***	
Upper	0.718 ***		0.84 ***		0.73 ***		0.69 **	
	FIN-CO_2				EC-CO_2			
Regimes:	1		2		1		2	
Lower	0.66 **		0.65 **		0.68 **		0.708 ***	
Upper	0.603 **		0.62 **		0.63 **		0.695 **	
	Diagnostic Tests							
LogL [2]	669.54		754.263		654.92		712.218	
AIC	−2.33		−4.77		−2.03		−4.06	
ARCH-LM	0.3129		0.497		0.3055		0.467	

[1] Stability condition: ARCH + GARCH < 1. [2] LogL is the log-likelihood, *p* is the *p*-value, AIC is the Akaike information criterion, and ARCH-LM is the Lagrange multiplier test statistic of the autoregressive conditional heteroskedasticity (ARCH) effects in the residuals of the model. *** and ** indicate statistical significance at 1% and 5% levels of significance, respectively.

Furthermore, copula parameters are estimated and presented for variable pairs in the last part of Table 9. The copula parameters are statistically significant for each pair and in each regime. For each variable pair in each regime, the parameter estimates range between 0.603 and 0.87, confirming the existence of moderate to high levels of positive tail dependence between the analyzed variables. In addition, the results also point to a significant level of asymmetry once the copula parameters are compared for the two distinct regimes, confirming nonlinearity in contagion in addition to the existence of tail dependence and contagion with variations depending on the type of regime examined.

4.9. Nonlinear Copula Granger Causality Test Results

The Granger causality test results obtained from the TAR-TR-GARCH–copula causality test are presented in Table 10. In the first row, the causality effects between BTC and CO_2 are examined. The results indicate that causality between Bitcoin and CO_2 emissions yields similar outcomes in both regimes 1 and 2, with evidence of unidirectional causality from Bitcoin to CO_2 emissions in both regimes. Although the direction of causality aligns with expectations, the findings highlight the causality effect regardless of whether it occurs during relatively low- or high-volatility regimes. Moving to the second part of Table 10, the causality between FIN and CO_2 emissions is assessed. The results of the causality test reveal unidirectional causality from Fintech to CO_2 in both regimes. Thus, irrespective of the regime type, unidirectional causality from Fintech to CO_2 emissions cannot be rejected.

Table 10. TAR-TR-GARCH–copula causality test results.

Tested Direction of Causality	Regime 1	Determined Direction	Regime 2	Determined Direction
$CO_2 \rightarrow$BTC	1.19 [1]	BTC$\rightarrow CO_2$	1.59	Unidirectional
BTC$\rightarrow CO_2$	3.85 ***	Unidirectional	4.88 ***	BTC$\rightarrow CO_2$
FIN$\rightarrow CO_2$	3.19 ***	Unidirectional	5.14 ***	Unidirectional
$CO_2 \rightarrow$FIN	1.26	FIN$\rightarrow CO_2$	1.26	FIN$\rightarrow CO_2$
BTC$\rightarrow$FIN	3.18 ***	Bi-directional	4.77 ***	Bi-directional
FIN$\rightarrow$BTC	2.88 ***		3.87 ***	
BTC$\rightarrow$EC	5.842 ***	Unidirectional	3.85 ***	Unidirectional
EC$\rightarrow$BTC	1.245	BTC$\rightarrow$EC	0.27	BTC$\rightarrow$EC
FIN$\rightarrow$EC	4.403 ***	Unidirectional	3.77 ***	Unidirectional
EC$\rightarrow$FIN	1.19	FIN$\rightarrow$EC	0.94	FIN$\rightarrow$EC
EC$\rightarrow CO_2$	3.56 ***	Unidirectional	3.098 ***	Unidirectional
$CO_2 \rightarrow$EC	1.008	EC$\rightarrow CO_2$	1.55	EC$\rightarrow CO_2$

[1] *t*-test statistics are reported. *** indicates statistical significance at 1% significance level.

Regime-specific Granger causality test results between BTC and FIN are presented in the second row of Table 10. The findings suggest that Granger causality can be rejected neither from FIN to BTC nor from BTC to FIN at a 1% level of statistical significance. Consequently, bidirectional Granger causality between the two series is acknowledged. Once the Granger causality in the context of threshold copula–GARCH regimes is examined for BTC and EC, the findings indicate strong evidence for Granger causality from Bitcoin to its energy consumption in both regimes. Similar unidirectional links also exist in both regimes, indicating Granger causality from Fintech to energy consumption in addition to Granger causality from Bitcoin. The Granger causality between energy consumption and CO_2 emissions is evaluated in the last part of Table 10, for which the test statistics are significant at a 1% level of statistical significance, and the findings confirm the existence of unidirectional Granger causality from EC to CO_2 in both regimes without distinction.

4.10. Discussion

The empirical analysis used a long sample of daily observations to evaluate various factors such as long-range dependence, entropy, complexity, persistence, mean reversion, chaos, tail dependence, contagion, and causality in Bitcoin, Fintech, energy consumption, and CO_2 emission concentrations. Methods including Hurst–Mandelbrot and Lo's scaled R/S tests; Shannon, HCT, Tsallis, and Rényi entropies; the Kolmogorov–Sinai complexity measure; the Hurst exponent; and the largest Lyapunov exponent measurement were employed. The findings of this study reveal complex relations of nonlinear and chaotic dynamics, regime-dependent causality, and long-range dependence between Bitcoin prices, Fintech markets, energy consumption, and CO_2 emission concentrations. These relationships are critical to understanding the unpredictable and intertwined nature of these variables, which have significant implications for both financial stability and environmental sustainability.

The key empirical findings are as follows:

1. *Nonlinear and Chaotic Dynamics.* The findings revealed evidence of entropy, fractionality, chaos, and complexity in the variables under investigation. Shannon, HCT, Tsallis, and Rényi entropy and Kolmogorov–Sinai complexity measures, along with positive Lyapunov exponents, confirm the chaotic nature and unpredictability of Bitcoin prices, Fintech markets, energy consumption, and CO_2 emission concentrations. The Kolmogorov–Sinai complexity metric further substantiates the existence of complex and unpredictable patterns, indicating a high degree of uncertainty and randomness in these series.
2. *Regime-dependent Asymmetric Causality and Contagion.* The TAR-TR-GARCH–copula causality approach reveals significant regime-dependent asymmetric tail dependence:
    - Strong positive tail dependence between Bitcoin, Fintech, energy consumption, and CO_2 emissions highlights the substantial contagion effects, particularly during extreme market conditions.
    - Significant regime-dependent Granger causality relations are determined as follows:
        - Unidirectional causality from Bitcoin to CO_2 emission concentrations;
        - Unidirectional causality from Fintech to CO_2 emission concentrations;
        - Bidirectional causality in both regimes between Bitcoin and Fintech markets, indicating feedback effects and underscoring the mutual influence and interdependence between these markets.
        - Unidirectional causality from energy consumption to CO_2 emission concentrations observed across both low- and high-volatility regimes;
3. *Long-range Dependence and Persistence.* Hurst exponents and the non-rejection of fractional difference parameters indicate long-range dependence and persistence in the level series of Bitcoin, Fintech markets, energy consumption of the Bitcoin network, and CO_2 emission concentrations. This persistence is particularly pronounced in the volatility series, suggesting that periods of high or low volatility are likely to be followed by similar periods. Further, findings of the study indicate evidence of mean reversion in the first-differenced series, particularly for CO_2 and Fintech, which exhibit tendencies towards anti-persistence.
4. *Complex and Nonlinear Contagion and Causality Relations Evident under Upper and Lower Tails.* The empirical findings confirmed the chaotic dynamics, underscoring the inherent unpredictability and complexity within these variables. Notably, the complex relations cannot be disregarded given the regime-dependent asymmetric causality and strong positive tail dependence at both the upper and lower tails of the datasets in regimes 1 and 2, the former characterized by low volatility and the latter by high volatility.

As a result, the findings highlight the significant level of contagion effects between the Bitcoin cryptocurrency market, the Fintech market, energy consumption of the Bitcoin network, and global environmental pollution proxied by CO_2 emission concentrations.

The regime-dependent causality relations combined with contagion and dependence at extreme levels of data captured under the lower and upper tails point to important effects of Bitcoin and Fintech and energy consumption on CO_2 emission concentrations, along with feedback effects between Bitcoin and Fintech. Additionally, the persistent long-range dependence and chaotic structures identified in the volatility series of these variables further support the intricate and dynamic nature of their interrelationships. The causality test results reveal nonlinear and unidirectional causal effects from Bitcoin to CO_2 emission concentrations in both regimes, confirming Bitcoin's ecological footprint as noted by [10]. Additionally, our econometric model estimates suggest positive parameter estimates for Bitcoin, coupled with positive tail dependence parameters, implying significant effects of Bitcoin on CO_2 emissions. Recently, [17] obtained regime-dependent and strongly positive tail dependence and contagion between Fintech, energy consumption, and CO_2 emissions. Bitcoin's sustainability issues are highlighted, given its substantial share in the global cryptocurrency market [11]. Moreover, our results showed that single-regime methods may yield incorrect or unreliable results. As emphasized by several studies, regime shifts and structural changes can lead to deviations when nonlinearity is present in the series. The results coincide with findings by Bildirici [50] and Kim et al. [22], highlighting the effectiveness of the copula–GARCH causality extension to regime-dependent nonlinear models and causality tests.

4.11. Policy Implications

Policy implications in the presence of chaotic structures, contagion, and causality require a multidimensional approach. Key steps include addressing nonlinear and chaotic dynamics, considering regime-dependent asymmetric causality and contagion, evaluating long-range dependence, and emphasizing complex contagion and causality relations.

Given the chaotic nature of Bitcoin prices, Fintech markets, energy consumption, and CO_2 emissions, policymakers should enhance risk management and monitoring to address sudden shifts. Traditional linear models are inadequate; regulatory frameworks must adapt to these complex dynamics with responsive interventions. During extreme market conditions, stricter, regime-specific policies are needed to manage heightened contagion and risk. Long-range dependence suggests that short-term measures can have lasting effects, requiring careful planning in environmental and energy policies. Nonlinear contagion and causality should inform policies that mitigate contagion risk with flexible regulatory approaches—stricter during high volatility and lenient in stable periods.

Significant causality from Bitcoin and Fintech to CO_2 emissions underscores the need to integrate environmental considerations into digital currency and Fintech regulation. This could include incentives for renewable energy use or penalties for high energy consumption. To manage persistence in Bitcoin, energy consumption, CO_2 emissions, and Fintech, mechanisms like dynamic energy tariffs may help reduce environmental impacts. Integrating environmental and financial policies is essential for effective regulation, balancing financial stability with environmental sustainability to address complex interdependencies identified in this study.

4.12. Characteristics of the Methods and Possible Directions for Future Research

The model given above has four distinct characteristics. First, it focuses on solving the problem of modeling contagion, tail dependence, and causality dynamics under nonlinearity. The model is not produced specifically to solve forecasting problems; however, the TAR-TR-GARCH models are shown to produce effective results for heteroskedastic and nonlinear time series [19]. The second characteristic is the sharp splitting of the regression space in capturing nonlinearity. The model structure captures the nonlinear splitting of the regression space specifically with the identity function, which is a similar treatment of the step function in the neural networks, which should be preferred for data modeling problems with sudden regime shifts. For neural network activation functions with smooth vs. sudden activations, readers are referred to [51]. In the case of series with smooth regime

transitions, smooth transition GARCH-type models can be used [52]. However, careful examination is necessary to check the existence of significance and the smoothness of the transition with appropriate tests by [53].

The third characteristic is the endogenous modeling of regime changes. The method assumes the regime splitting to be determined endogenously as a function of the current or the lagged shocks, residuals, or variables. For models that assume regime switches as an exogenous Markov chain, a Markov-switching treatment of nonlinear copula GC exists [25]. The fourth characteristic is that, as in many approaches, all variables are in the same frequency, and in this study, they were in a daily frequency. Recent developments in GARCH proposed modeling data with mixed data sampling (MIDAS) [54]. Recently, the GARCH-MIDAS model has been generalized to long short-term model (LSTM) deep neural networks with the proposed hybrid GARCH-MIDAS-LSTM model [55] to solve forecasting problems.

Following the discussion above, a set of future directions is suggested. First, the methods used in this study focus on determining chaos, entropy, fractionality, and nonlinearity characteristics, followed by focusing on the modeling problem of nonlinearity, tail dependence, contagion, and Granger causality dynamics with TAR-TR-GARCH–copula causality methods. In the case of problems specifically focusing on forecasting the future direction of nonlinear contagion, tail dependence, and causality, future studies should consider integrating neural network GARCH modeling suggested by [56] and generalized to a family of nonlinear NN-GARCH by [57] and to LSTM-GARCH models [55,58] with the applied models in this study. For future studies that specifically aim at producing future forecasts for contagion and causality dynamics with datasets subject to mixed sampling frequencies, a suggested direction is to integrate the GARCH-MIDAS-LSTM model [55] with TAR-TR-GARCH–copula causality methods.

5. Conclusions

The study's aims are two-fold. The first is the examination of structures embedded in daily Bitcoin, Fintech, energy consumption, and global CO_2 emission concentrations, characterized by entropy, fractionality, long-range dependence, complexity, chaos, persistence, and mean reversion in addition to nonlinearity and heteroskedasticity. The second is, after the determination of the above-mentioned factors, the modeling of the marginal and joint processes of Bitcoin, Fintech, energy consumption, and global CO_2 emissions. For this purpose, the variables are modeled with TAR-TR-GARCH–copula causality methods, which simultaneously capture the conditional mean as a threshold autoregressive and the conditional variance as threshold generalized autoregressive conditional heteroskedasticity, which encounters regime-dependent nonlinearity in the analyzed series. Following the modeling of the marginals, joint relations are modeled for contagion, tail dependence, and causality within the TAR-TR-GARCH–copula causality framework.

In the empirical analysis, by employing a long sample consisting of daily observations covering the period from 25 June 2012 to 22 June 2024, the variables are tested with Hurst–Mandelbrot and Lo's scaled R/S tests to evaluate long-range dependence; Shannon, HCT, Tsallis, and Rényi entropies and entropic index; Kolmogorov–Sinai measure for complexity; Kantz and Rosenstein et al.'s methods for largest Lyapunov exponent measurement; and Hurst exponent to examine the degree of persistence and mean reversion and chaos in daily Bitcoin and Fintech, energy consumption, and CO_2 emissions for the level and first-differenced forms of the dataset. Afterward, the variables are evaluated for nonlinearity with the BDS test and ARCH-type heteroskedasticity with the ARCH-LM tests. The findings are listed below. The overlook suggests that these findings provide the basis for modeling the complex structures of and interdependencies between the analyzed variables with recent TAR-TR-GARCH–copula causality methods. As mentioned above, modeling marginals with TAR-TR-GARCH processes and joint relations with copula and causality relations with the generalized Granger causality method provides vital insights regarding

the regime-dependent contagion and causality relations, in addition to determining the directional flows of causality between the analyzed variables.

The analysis reveals entropy, fractionality, chaos, and complexity in Bitcoin prices, Fintech markets, energy consumption, and CO_2 emissions. Shannon, HCT, Tsallis, and Rényi entropies and the Kolmogorov–Sinai complexity measure, along with positive Lyapunov exponents, confirm the chaotic and unpredictable nature of these variables. The Kolmogorov–Sinai complexity metric further highlights the high degree of uncertainty and randomness present. The TAR-TR-GARCH–copula causality approach shows significant regime-dependent asymmetric tail dependence. Strong positive tail dependence between Bitcoin, Fintech, energy consumption, and CO_2 emissions indicates substantial contagion effects, especially during extreme market conditions. Hurst exponents and fractional difference parameters indicate long-range dependence and persistence in Bitcoin, energy consumption, CO_2 emissions, and Fintech, particularly in volatility series. There is also evidence of mean reversion in the first-differenced series, especially for CO_2 and Fintech, which tend to exhibit anti-persistence. The study confirms chaotic dynamics, emphasizing the inherent unpredictability and complexity within these variables. The regime-dependent asymmetric causality and strong positive tail dependence at both upper and lower tails underscore significant contagion effects between the Bitcoin market, the Fintech market, energy consumption of the Bitcoin network, and global CO_2 emissions. The persistent long-range dependence and chaotic structures in the volatility series further highlight the intricate and dynamic nature of these interrelationships. The TAR-TR-GARCH–copula causality approach shows significant regime-dependent asymmetric tail dependence. Strong positive tail dependence between Bitcoin, Fintech, energy consumption, and CO_2 emissions indicates substantial contagion effects, especially during extreme market conditions. Further, key causality findings are unidirectional causality from Bitcoin, Fintech, and energy consumption to CO_2 emissions in both low- and high-volatility regimes, coupled with bidirectional causality between Bitcoin and Fintech, suggesting mutual influence and interdependence.

In summary, this study provides a comprehensive examination of the nonlinear and chaotic dynamics linking Bitcoin, Fintech, energy consumption, and CO_2 emissions, and the econometric methods employed reveal crucial insights into the regime-specific causality and contagion effects, offering a robust framework for understanding these relationships. Based on these findings, policymakers should consider chaos, long-range dependence, and nonlinearity in Bitcoin, Fintech, energy consumption, and CO_2 emissions and their outcomes in policymaking processes. Therefore, policymakers must consider more drastic measures to address the environmental impacts of the growing cryptocurrency market. The study underscores the need for a multifaceted policy approach that accounts for the chaotic dynamics, long-range dependence, and complex interdependencies identified in these variables. Policymakers must be prepared to manage the inherent unpredictability and contagion risks associated with Bitcoin, Fintech, and their environmental impacts. This requires a dynamic and flexible regulatory framework that can adapt to changing market conditions while also addressing the broader implications for global sustainability. The findings also suggest that further research is needed to explore the potential for mitigating these risks through more sophisticated modeling and regulatory strategies.

Author Contributions: Conceptualization, M.E.B.; methodology, M.E.B., Ö.Ö.E. and Y.U.; software, M.E.B., Ö.Ö.E. and Y.U.; validation, M.E.B., Ö.Ö.E. and Y.U.; formal analysis, M.E.B., Ö.Ö.E. and Y.U.; investigation, M.E.B., Ö.Ö.E. and Y.U.; resources, M.E.B., Ö.Ö.E. and Y.U.; data curation, M.E.B., Ö.Ö.E. and Y.U.; writing—original draft preparation, M.E.B., Ö.Ö.E. and Y.U.; writing—review and editing, M.E.B., Ö.Ö.E. and Y.U.; visualization, M.E.B., Ö.Ö.E. and Y.U.; supervision, M.E.B.; project administration, M.E.B., Ö.Ö.E. and Y.U.; funding acquisition, M.E.B., Ö.Ö.E. and Y.U. All authors have read and agreed to the published version of the manuscript.

Funding: This research received no external funding.

Data Availability Statement: Datasets are available from public depositories as detailed in Section 3.1.

Conflicts of Interest: The authors declare no conflicts of interest.

Nomenclature

ARCH	Autoregressive conditional heteroskedasticity
AIC	Akaike information criterion
ARCH-LM	Lagrange multiplier test statistic for ARCH effects
BDS	Brock, Deckert, and Scheinkman independence and nonlinearity test
BTC	Bitcoin price
CO_2	Global carbon dioxide emissions
EC	Energy consumption from the Bitcoin network
FIN	Global Fintech stock index
GARCH	Generalized autoregressive conditional heteroskedasticity
HCT	Havdra–Charvat–Tsallis entropy
LogL	Log-likelihood
LSTM	Long short-term memory deep neural networks
NN-GARCH	Neural networks–GARCH
R/S	Range/scale test
SIC	Schwarz information criterion
TAR-TR-GARCH–copula causality	Threshold autoregressive-threshold-generalized autoregressive conditional heteroskedasticity–copula causality

References

1. Lorenz, E.N. Deterministic Nonperiodic Flow. *J. Atmos. Sci.* **1963**, *20*, 130–141. [CrossRef]
2. Ruelle, D.; Takens, F. On the Nature of Turbulence. *Commun. Math. Phys.* **1971**, *20*, 167–192. [CrossRef]
3. Guckenheimer, J.; Holmes, P. *Nonlinear Oscillations, Dynamical Systems, and Bifurcations of Vector Fields*; Springer: Berlin/Heidelberg, Germany, 1983; Volume 42. [CrossRef]
4. Kumar, U.; Prakash, A.; Jain, V.K. Characterization of Chaos in Air Pollutants: A Volterra–Wiener–Korenberg Series and Numerical Titration Approach. *Atmos. Env.* **2008**, *42*, 1537–1551. [CrossRef]
5. Yu, B.; Huang, C.; Liu, Z.; Wang, H.; Wang, L. A Chaotic Analysis on Air Pollution Index Change over Past 10 Years in Lanzhou, Northwest China. *Stoch. Environ. Res. Risk Assess.* **2011**, *25*, 643–653. [CrossRef]
6. Chakraborty, A.; Veeresha, P. Effects of Global Warming, Time Delay and Chaos Control on the Dynamics of a Chaotic Atmospheric Propagation Model within the Frame of Caputo Fractional Operator. *Commun. Nonlinear Sci. Numer. Simul.* **2024**, *128*, 107657. [CrossRef]
7. Bildirici, M.E. Chaotic Dynamics on Air Quality and Human Health: Evidence from China, India, and Turkey. *Nonlinear Dyn. Psychol. Life Sci.* **2021**, *25*, 207–236.
8. Ucan, Y.; Bildirici, M. Air Temperature Measurement Based on Lie Group SO(3). *Therm. Sci.* **2022**, *26*, 3089–3095. [CrossRef]
9. de Vries, A. Bitcoin's Energy Consumption Is Underestimated: A Market Dynamics Approach. *Energy Res. Soc. Sci.* **2020**, *70*, 101721. [CrossRef]
10. de Vries, A.; Gallersdörfer, U.; Klaaßen, L.; Stoll, C. Revisiting Bitcoin's Carbon Footprint. *Joule* **2022**, *6*, 498–502. [CrossRef]
11. de Vries, A. Renewable Energy Will Not Solve Bitcoin's Sustainability Problem. *Joule* **2019**, *3*, 893–898. [CrossRef]
12. Wendl, M.; Doan, M.H.; Sassen, R. The Environmental Impact of Cryptocurrencies Using Proof of Work and Proof of Stake Consensus Algorithms: A Systematic Review. *J. Env. Manag.* **2023**, *326*, 116530. [CrossRef] [PubMed]
13. Kohli, V.; Chakravarty, S.; Chamola, V.; Sangwan, K.S.; Zeadally, S. An Analysis of Energy Consumption and Carbon Footprints of Cryptocurrencies and Possible Solutions. *Digit. Commun. Netw.* **2023**, *9*, 79–89. [CrossRef]
14. Digiconomist Bitcoin Energy Consumption Index—Digiconomis. Available online: https://digiconomist.net/bitcoin-energy-consumption (accessed on 14 March 2023).
15. Badea, L.; Mungiu-Pupazan, M.C. The Economic and Environmental Impact of Bitcoin. *IEEE Access* **2021**, *9*, 48091–48104. [CrossRef]
16. Jiang, S.; Li, Y.; Lu, Q.; Hong, Y.; Guan, D.; Xiong, Y.; Wang, S. Policy Assessments for the Carbon Emission Flows and Sustainability of Bitcoin Blockchain Operation in China. *Nat. Commun.* **2021**, *12*, 1–10. [CrossRef]
17. Ersin, Ö.Ö.; Bildirici, M.E. Are Cleaner Energy and Financial Technologies Needed? Contagion and Causality Evidence between Global Fintech Markets, Energy Consumption, and Environmental Pollution. *Clean. Technol. Env. Policy* **2024**, 1–15. [CrossRef]
18. Bildirici, M. The Chaotic Behavior among the Oil Prices, Expectation of Investors and Stock Returns: TAR-TR-GARCH Copula and TAR-TR-TGARCH Copula. *Pet. Sci.* **2019**, *16*, 217–228. [CrossRef]
19. Bildirici, M.; Ersin, O.; Onat, I.Ş. Examination of the Predictability of BDI and VIX: A Threshold Approach. *Int. J. Transp. Econ.* **2019**, *XLVI*, 9–28. [CrossRef]

20. Hansen, B.E. Sample Splitting and Threshold Estimation. *Econometrica* **2000**, *68*, 575–603. [CrossRef]
21. Boubaker, H.; Sghaier, N.; Boubaker, H.; Sghaier, N. Markov-Switching Time-Varying Copula Modeling of Dependence Structure between Oil and GCC Stock Markets. *Open J. Stat.* **2016**, *6*, 565–589. [CrossRef]
22. Kim, J.M.; Lee, N.; Hwang, S.Y. A Copula Nonlinear Granger Causality. *Econ. Model.* **2020**, *88*, 420–430. [CrossRef]
23. Granger, C.W.J. Investigating Causal Relations by Econometric Models and Cross-Spectral Methods. *Econometrica* **1969**, *37*, 424. [CrossRef]
24. Bildirici, M.E.; Salman, M.; Ersin, Ö.Ö. Nonlinear Contagion and Causality Nexus between Oil, Gold, VIX Investor Sentiment, Exchange Rate and Stock Market Returns: The MS-GARCH Copula Causality Method. *Mathematics* **2022**, *10*, 4035. [CrossRef]
25. Bildirici, M.; Ersin, Ö.Ö.; Ibrahim, B. Chaos, Fractionality, Nonlinear Contagion, and Causality Dynamics of the Metaverse, Energy Consumption, and Environmental Pollution: Markov-Switching Generalized Autoregressive Conditional Heteroskedasticity Copula and Causality Methods. *Fractal Fract.* **2024**, *8*, 114. [CrossRef]
26. Hurst, H.E. Long-Term Storage Capacity of Reservoirs. *Trans. Am. Soc. Civ. Eng.* **1951**, *116*, 770–799. [CrossRef]
27. Mandelbrot, B.B. Statistical Methodology for Nonperiodic Cycles: From the Covariance to R/S Analysis. *Ann. Econ. Soc. Meas.* **1972**, *1*, 259–290.
28. Mandelbrot, B.B.; Wallis, J.R. Robustness of the Rescaled Range R/S in the Measurement of Noncyclic Long Run Statistical Dependence. *Water Resour. Res.* **1969**, *5*, 967–988. [CrossRef]
29. Lo, A.W. Long-Term Memory in Stock Market Prices. *Econometrica* **1991**, *59*, 1279. [CrossRef]
30. Andrews, D.W.K. Heteroskedasticity and Autocorrelation Consistent Covariance Matrix Estimation. *Econometrica* **1991**, *59*, 817. [CrossRef]
31. Geweke, J.; Porter-Hudak, S. The Estimation and Application of Long Memory Time Series Models. *J. Time Ser. Anal.* **1983**, *4*, 221–238. [CrossRef]
32. Phillips, P. *Discrete Fourier Transforms of Fractional Processes*; Cowles Foundation Discussion Papers; Emerald Group Publishing Limited: Leeds, UK, 1999.
33. Shannon, C.E. A Mathematical Theory of Communication. *Bell Syst. Tech. J.* **1948**, *27*, 379–423. [CrossRef]
34. Rényi, A. On Measures of Entropy and Information. In Proceedings of the Berkeley Symposium on Mathematical Statistics and Probability, 20 June–30 July 1960; Neyman, J., Ed.; University of California Press: Berkeley, CA, USA, 1961; Volume 4.1, pp. 547–562.
35. Tsallis, C. Possible Generalization of Boltzmann-Gibbs Statistics. *J. Stat. Phys.* **1988**, *52*, 479–487. [CrossRef]
36. Havrda, J.; Charvât, F. Quantification Method of Classification Processes Concept of Structural «-Entropy. *Kybernetica* **1967**, *3*, 30–35.
37. Tsallis, C.; Mendes, R.S.; Plastino, A.R. The Role of Constraints within Generalized Nonextensive Statistics. *Phys. A Stat. Mech. Appl.* **1998**, *261*, 534–554. [CrossRef]
38. Baptista, M.S.; Ngamga, E.J.; Pinto, P.R.F.; Brito, M.; Kurths, J. Kolmogorov–Sinai Entropy from Recurrence Times. *Phys. Lett. A* **2010**, *374*, 1135–1140. [CrossRef]
39. Kantz, H. A Robust Method to Estimate the Maximal Lyapunov Exponent of a Time Series. *Phys. Lett. A* **1994**, *185*, 77–87. [CrossRef]
40. Rosenstein, M.T.; Collins, J.J.; De Luca, C.J. A Practical Method for Calculating Largest Lyapunov Exponents from Small Data Sets. *Phys. D* **1993**, *65*, 117–134. [CrossRef]
41. Brock, W.A.; Dechert, W.D.; Scheinkman, J.A. *A Test for Independence Based on the Correlation Dimension*; University of Wisconsin, Social Systems Research Unit: Madison, WI, USA, 1987.
42. Kwiatkowski, D.; Phillips, P.C.B.; Schmidt, P.; Shin, Y. Testing the Null Hypothesis of Stationarity against the Alternative of a Unit Root: How Sure Are We That Economic Time Series Have a Unit Root? *J. Econ.* **1992**, *54*, 159–178. [CrossRef]
43. Kapetanios, G.; Shin, Y.; Snell, A. Testing for a Unit Root in the Nonlinear STAR Framework. *J. Econ.* **2003**, *112*, 359–379. [CrossRef]
44. Engle, R.F. Autoregressive Conditional Heteroscedasticity with Estimates of the Variance of United Kingdom Inflation. *Econometrica* **1982**, *50*, 987. [CrossRef]
45. Kaspar, F.; Schuster, H.G. Easily Calculable Measure for the Complexity of Spatiotemporal Patterns. *Phys. Rev. A* **1987**, *36*, 842. [CrossRef]
46. Masthay, M.; Benton, C.; Guerrieri, L.; Keil, R.; Masthay, M.; Benton, C.; Guerrieri, L.; Keil, R. The Tsallis Entropic Index as a Measure of Distance from Thermal Equilibrium in Paramagnetic Spin Lattices. In *Nanomaterials and Nanostructures—Annual*; IntechOpen: London, UK, 2024; Volume 2024, ISBN 978-0-85014-199-3.
47. Beran, J. On a Class of M-Estimators for Gaussian Long-Memory Models. *Biometrika* **1994**, *81*, 755–766. [CrossRef]
48. Wolf, A.; Swift, J.B.; Swinney, H.L.; Vastano, J.A. Determining Lyapunov Exponents from a Time Series. *Phys. D* **1985**, *16*, 285–317. [CrossRef]
49. Feldman, D.P.; Crutchfield, J.P. Measures of Statistical Complexity: Why? *Phys. Lett. A* **1998**, *238*, 244–252. [CrossRef]
50. Bildirici, M.E. Chaos Structure and Contagion Behavior between COVID-19, and the Returns of Prices of Precious Metals and Oil: MS-GARCH-MLP Copula. *Nonlinear Dyn. Psychol. Life Sci.* **2022**, *26*, 209–230.
51. Bishop, C. *Neural Networks for Pattern Recognition*, 1st ed.; Oxford University Press: New York, NY, USA, 1995; Volume 5, ISBN 9780198538646.
52. González-Rivera, G. Smooth-Transition GARCH Models. *Stud. Nonlinear Dyn. Econom.* **1998**, *3*. [CrossRef]

53. Teräsvirta, T. Specification, Estimation, and Evaluation of Smooth Transition Autoregressive Models. *J. Am. Stat. Assoc.* **1994**, *89*, 208–218. [CrossRef]
54. Conrad, C.; Custovic, A.; Ghysels, E. Long- and Short-Term Cryptocurrency Volatility Components: A GARCH-MIDAS Analysis. *J. Risk Financ. Manag.* **2018**, *11*, 23. [CrossRef]
55. Ersin, Ö.Ö.; Bildirici, M. Financial Volatility Modeling with the GARCH-MIDAS-LSTM Approach: The Effects of Economic Expectations, Geopolitical Risks and Industrial Production during COVID-19. *Mathematics* **2023**, *11*, 1785. [CrossRef]
56. Donaldson, R.G.; Kamstra, M. An Artificial Neural Network-GARCH Model for International Stock Return Volatility. *J. Empir. Financ.* **1997**, *4*, 17–46. [CrossRef]
57. Bildirici, M.; Ersin, Ö.Ö. Improving Forecasts of GARCH Family Models with the Artificial Neural Networks: An Application to the Daily Returns in Istanbul Stock Exchange. *Expert. Syst. Appl.* **2009**, *36*, 7355–7362. [CrossRef]
58. Hu, Y.; Ni, J.; Wen, L. A Hybrid Deep Learning Approach by Integrating LSTM-ANN Networks with GARCH Model for Copper Price Volatility Prediction. *Phys. A Stat. Mech. Appl.* **2020**, *557*, 124907. [CrossRef]

Disclaimer/Publisher's Note: The statements, opinions and data contained in all publications are solely those of the individual author(s) and contributor(s) and not of MDPI and/or the editor(s). MDPI and/or the editor(s) disclaim responsibility for any injury to people or property resulting from any ideas, methods, instructions or products referred to in the content.